ACS APPLIED MATERIALS & INTERFACES

Research Article

Cite This: ACS Appl. Mater. Interfaces 2018, 10, 36711−36720

www.acsami.org

Omniphilic Polysaccharide-Based Nanocarriers for Modular Molecular Delivery in a Broad Range of Biosystems

Roi Rutenberg,[†,‡] Daria Galaktionova,[§] Gilad Golden,[†,†] Yael Cohen,[†,∥] Yael Levi-Kalisman,[⊥] Guy Cohen,[#] Petr Král,[§,¶] and Elena Poverenov*[,†]

[†]Postharvest and Food Science Institute, Agricultural Research Organization, The Volcani Center, Rishon LeZion 50250, Israel

[‡]Institute of Biochemistry, Food Science and Nutrition, Faculty of Agriculture, Food and Environment and [∥]Environmental Studies and Agricultural Resources, Faculty of Agriculture, Food and Environment, The Hebrew University of Jerusalem, Rehovot 76100, Israel

[§]Department of Chemistry, University of Illinois at Chicago, Chicago 60607, Illinois, United States

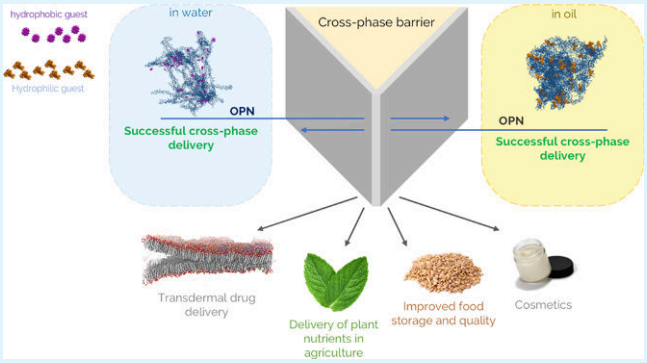
[⊥]The Center for Nanoscience and Nanotechnology, and the Silberman Institute for Life Sciences, The Hebrew University of Jerusalem, Jerusalem 91904, Israel

[#]The Skin Research Institute, Dead Sea & Arava Science Center, Masada 86910, Israel

[¶]Departments of Physics and Biopharmaceutical Sciences, University of Illinois at Chicago, Chicago 60607, Illinois, United States

Supporting Information

ABSTRACT: Self-adjusting omniphilic nanocarriers (OPNs) with a multisolvent aptitude were prepared via a Schiff base reaction between chitosan, a natural polysaccharide, and bioactive aldehydes. Experimental studies supported by atomistic molecular dynamics simulations revealed these OPNs can encapsulate insoluble molecular cargo, transport them in aqueous or lipid environments, and deliver them through cross-phase barriers. N-imine dynamic covalent bonds have been incorporated to endow the OPNs with pH responsiveness, also allowing the amplification of their bioactivity, as demonstrated in vitro with the ability to delay fungal proliferation in wheat grains. The reported OPNs hold remarkable potential as biocompatible nanocarriers for the effective delivery of active agents in agriculture, medicine, and cosmetics.



KEYWORDS: *omniphilic, cross-phase delivery, self-assembly, polysaccharide, atomistic molecular dynamics simulations, pH responsive release*

INTRODUCTION

In the past two decades, numerous types of nanocarriers based on biocompatible polymers and nanoparticles were developed and utilized for molecular delivery in medicine,[1] food, and cosmetics.[2−5] Among various biopolymers suitable for building nanocarriers, polysaccharides are of particular interest, because of their low price, availability, hypoallergenic properties, and well-defined chemical structures that allow their rational modifications.[6,7] Biopolymers were widely utilized for the delivery of hydrophobic compounds in aqueous solutions.[8,9] A complementary delivery of hydrophilic compounds in lipophilic environments was much less explored, although it is also highly beneficial in numerous fields.

Significant delivery problems arise when the molecular cargo needs to be transferred from one phase to another across a barrier of a different nature. For example, transdermal delivery is an attractive alternative to oral delivery and hypodermic injections. It has been employed for providing hydrophobic active agents, such as nicotine, lidocaine, and hormones,[10] whereas delivering hydrophilic compounds (such as insulin, antihistamines, hydrophilic antibiotics, and more) through the lipophilic skin barrier is challenging.[11,12] The cross-phase delivery problem is well known in agriculture, where fertilizers, nutrients, and protective agents are mostly hydrophilic and cannot be delivered to plants, as they are repelled by the hydrophobic cuticle that covers the epidermis of plant leaves.[13]

In this work, we have developed biopolymer-based nanocarriers that can encapsulate both hydrophobic and hydrophilic molecular cargo, transport them into either aqueous or lipid environments, and deliver them across different phases. These nanocarriers were entitled omniphilic, as in "like everything" in order to illustrate their aptitude toward various guest

Received: August 1, 2018
Accepted: October 4, 2018
Published: October 4, 2018

Downloaded via UNIV OF ILLINOIS CHICAGO on November 9, 2018 at 01:34:22 (UTC).
See https://pubs.acs.org/sharingguidelines for options on how to legitimately share published articles.

© 2018 American Chemical Society

DOI: 10.1021/acsami.8b12855
ACS Appl. Mater. Interfaces 2018, 10, 36711−36720

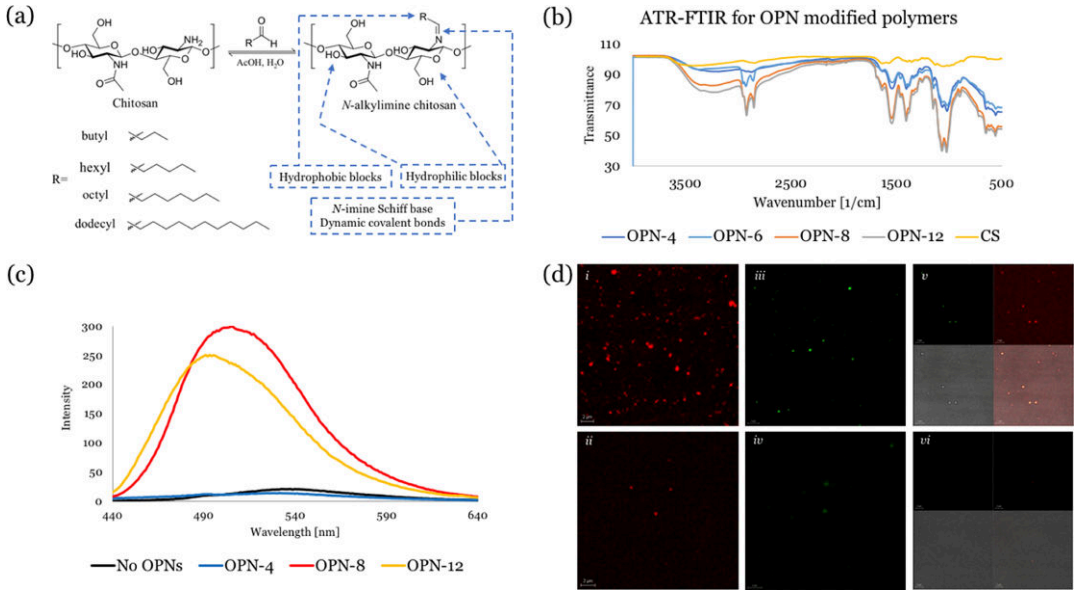


Figure 1. (a) Schematic illustration of OPNs synthesis. (b) FTIR of OPNs. (c) Spectrofluorometric scans of curcumin when presented to aqueous solutions of various OPNs. (d) CLSM images of RB, pyrene, and both probes simultaneously encapsulated by OPN-12 (i, iii, v, respectively) and corresponding images less than 60 s after application of an acidic stimulus (ii, iv, vi, respectively); scale bars are 2 μm.

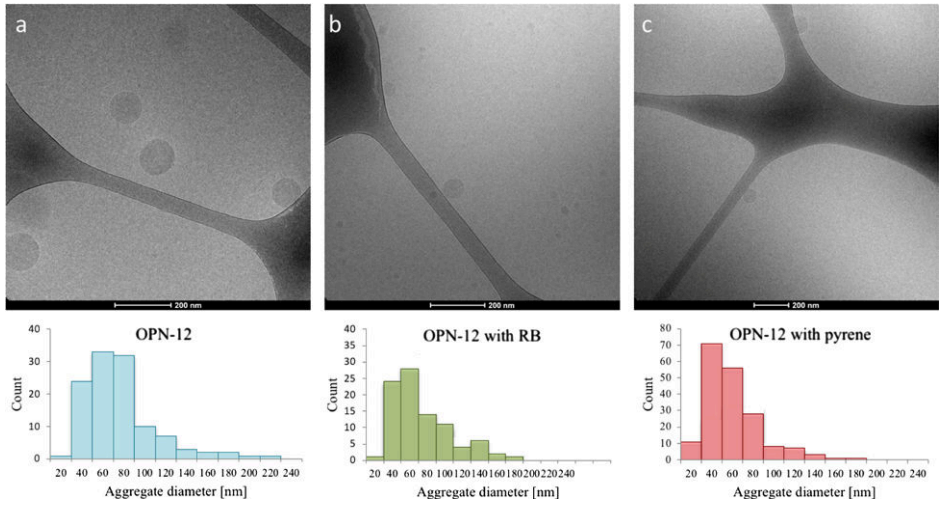


Figure 2. Cryo-TEM images and corresponding histograms for OPN-12 aggregates self-assembled in water with (a) no guest, (b) RB, and (c) pyrene molecules. Scale bar = 200 nm. Their histograms corresponding to each sample are shown below the images, calculated based on the measurements of over 200 individual aggregates.

molecules and solvent environments. Chitosan (CS), a natural polysaccharide known for its bioactivity,[14,15] was coupled to a series of natural aliphatic aldehydes endowed with bioactive properties.[16] The modified biopolymers were found to self-assemble into stable nano-aggregates, in both hydrophilic and hydrophobic environments, while encapsulating a molecular cargo. These omniphilic polysaccharide-based nanocarriers (OPNs) can be activated by their pH-responsive N-imine dynamic covalent bonds. This feature allows for a controlled release of their encapsulated cargo, and the OPNs' entire bioactive composition, thus affecting any target with multiple active agents, amplifying the overall activity.

RESULTS AND DISCUSSION

OPNs in an Aqueous Environment. CS was coupled with aliphatic aldehydes (4, 6, 8, or 12 carbons long) via a Schiff base reaction,[17] yielding a series of N-alkylimine nano-sized modified polysaccharides termed OPN-4, OPN-6, OPN-8, and OPN-12, respectively (Figure 1a). Fourier transform infrared (FTIR) scans have indicated the N-imine bond formation (1637 cm^{-1}) and the coupled aliphatic chains (2850−3000 cm^{-1}) with no traces of free aldehydes (Figure 1b).

The introduced hydrophobicity brought on with the conjugated aldehydes, along with the hydrophilic nature of CS, has enabled the formation of amphiphilic copolymers that self-assemble into submicron aggregates. Their critical aggregate concentrations (CACs) in water were measured using a spectrofluorometric method[18] and verified by dynamic light scattering (DLS) scans. As expected, the N-imine aldehyde coupling has lowered the CACs in accordance with the aliphatic chain length (0.21, 0.13, 0.02, and 6.01 × 10^{-3} mg/mL for OPN-4, 6, 8, and 12, respectively).

DOI: 10.1021/acsami.8b12855
ACS Appl. Mater. Interfaces 2018, 10, 36711−36720

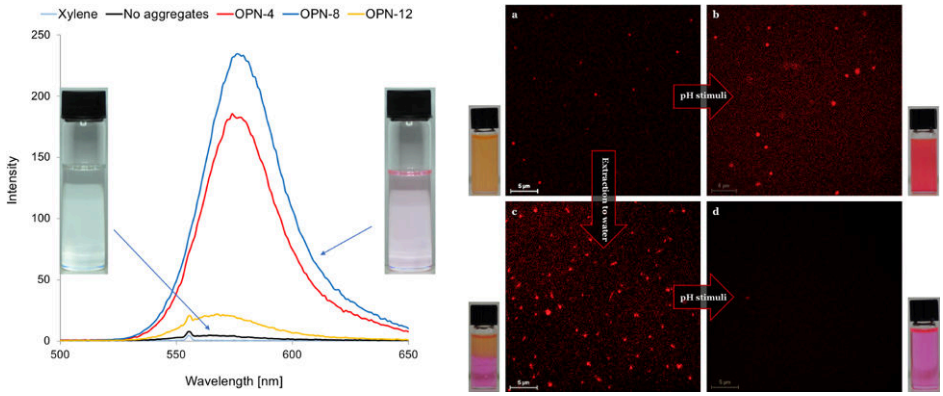


Figure 3. (left) Spectrofluorometric scans of RB in xylene with and without OPNs. (right) (a) CSLM images of OPN-4 and RB (a) in sunflower oil, (b) in sunflower oil after an acidic stimulus, (c) when extracted from oil to water, (d) in water after an acid stimulus.

Curcumin, a natural bioactive agent,[19] was used to verify the OPNs' ability to encapsulate and deliver hydrophobic compounds in an aqueous solution (Figure 1c). Rhodamine B (RB) and pyrene were then used as hydrophilic and hydrophobic fluorescent probes, respectively, and added to the OPN aqueous solutions with their encapsulation examined using confocal laser scanning microscopy (CLSM). Both systems formed sphere-shaped submicron aggregates, which displayed a prolonged Brownian motion in solution, indicating thermodynamic stability with no apparent agglomeration. When the RB and pyrene probes were added together, CLSM images revealed the fluorescent signals from both probes emanate from the same points of origin, indicating the OPNs can simultaneously house both hydrophilic and hydrophobic probes [Figure 1d(i,iii,v) for OPN-12, and Figure S3 for OPN-4 and OPN-8]. The prepared aggregates thus demonstrated a dual-housing capability for diverse guest types, deliverable either individually or concurrently.

The OPNs were designed to contain a pH stimuli-responsive N-imine dynamic covalent bond,[20,21] giving the possibility of a controlled OPN disassembly,[22] and consequent accelerated release of the coupled aldehydes together with the encapsulated payload. When an external pH stimulus was applied in tested OPNs, the fluorescent guest signals disappeared in all CLSM images [Figure 1d(ii,iv,vi)], pointing to the OPNs disassembly and subsequent release of the encapsulated dyes. It is worth noting the dynamic N-imine bond can be reduced to a steady secondary amine bond, when nonresponsive highly stable delivery systems are desired.[23]

Direct cryo-transmission electron microscopy (TEM) imaging revealed that payload-free OPN-12 solvated in water formed spherical assemblies with an average diameter of 79.5 nm (Figure 2). The encapsulation of the hydrophilic RB probe caused a slight size reduction in the assemblies to 74.2 nm, whereas encapsulating pyrene as a hydrophobic probe resulted in complexes with an average diameter of 63.8 nm. Atomistic molecular dynamics (MD) simulations have revealed this size decrease is caused by tighter packing of the complex through the encapsulated hydrophobic guest (see later).

OPNs in a Lipophilic Environment. The concentrated OPN aqueous solutions were added to xylene, an organic lipophilic solvent, and the mixtures were heated to remove the water fraction, leaving OPNs in the organic phase. DLS scans evidenced the presence of self-assembled nanostructures in xylene. In contrast to aqueous solutions, OPNs with longer side chains had higher CACs (0.48, 0.09, and 0.02 mg/mL for OPN-12, 8, and 4, respectively), showing that hydrophilic biopolymers with shorter side chains have a stronger driving force to aggregate in hydrophobic solvents. Using the same method of removing the water fraction from a binary solution, OPNs were transferred to sunflower oil, a lipophilic medium that resembles physiological lipid environments.[24]

The hydrophobic probes, pyrene and curcumin have been successfully encapsulated by OPNs in a lipid environment (Figures S6–S8). A hydrophilic payload, RB was encapsulated by OPNs. The control experiments had shown RB is insoluble on its own in these solvents. In the presence of OPNs, RB dissolves in these solvents as was shown by spectrofluorometric scans in xylene and by the appearance of a stable pink–violet color in either xylene or sunflower oil. This color had persisted for months as the glass vials in which this experiment was conducted were kept in dark and cool conditions so as not to bleach the fluorescent probe. Spectrofluorometric studies have revealed that OPN-4 or OPN-8 had a more significant effect on RB's fluorescent spectra than OPN-12 (Figure 3 left). CLSM images of RB-loaded OPNs in sunflower oil have demonstrated their long-term stability (Figure 3a). Unlike the case in aqueous media, no N-imine cleavage was achieved under lipid conditions even upon introducing an acidic stimulus, neither with a protic glacial acetic acid nor with $AlCl_3$ as a Lewis acid (Figure 3b).

Remarkably, the prepared OPNs were able to transport the encapsulated active agents across different phases. Whenever OPNs present in a lipid environment were exposed to an aqueous microenvironment, their migration back to the aqueous phase had occurred spontaneously. Once the hydrophilic compounds embedded OPNs arrive to the aqueous environment, their tendency to release any cargo is inherently increased (as is also further shown by atomistic MD simulations). However, a considerable amount of RB remains encapsulated in the OPNs (Figure 3c). Similarly, the OPN-encapsulated hydrophobic molecules were also observed in lipid solvents (Figures S6–S8). This remarkable ability of the OPNs to host various guests in different environments stems from their structural plasticity. Unlike other amphiphilic structures, OPNs do not have strictly defined hydrophobic or hydrophilic areas, but adaptive macrostructure that can concurrently adjust to different micropolarities. This feature endows the OPNs with an ability to create numerous favorable surroundings for different cargos and allows encapsulating hydrophilic molecules to a certain degree in a hydrophilic solvent and hydrophobic molecules in a lipid environment.

DOI: 10.1021/acsami.8b12855
ACS Appl. Mater. Interfaces 2018, 10, 36711–36720

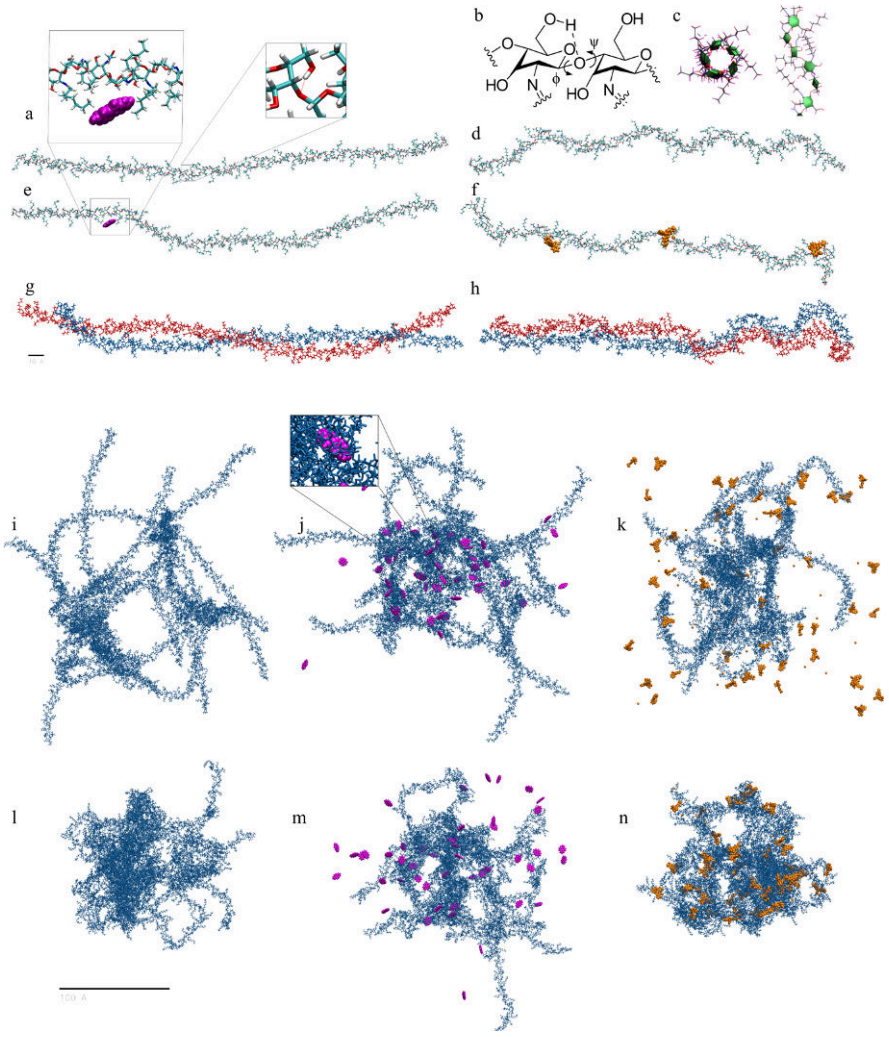


Figure 4. (a) One OPN-8 polysaccharide chain in water (after 15 ns of simulations). (Inset) Hydrogen bonding between H06 and linkage oxygen. (b) Chair configuration of a disaccharide with ψ and ϕ torsional angles shown. (c) Schematic representation of the helical structure of OPN-8 molecule. (d) Same as a) in *p*-xylene. (e) Same as (a) with 3 pyrene molecules (unbound pyrenes were deleted). (Inset) Detail of pyrene binding. (f) Same as (d) with 3 RB molecules. (g) Two chains from (a) in water (15 ns). (h) Two chains from (d) in *p*-xylene. (i) 10 chains in water (60 ns). (j) Same as (i) with 48 pyrene molecules (60 ns). (k) Same as (i) with 48 RB molecules (50 ns). (l–n) Same as (i–k) in *p*-xylene.

Notably, once the OPNs have returned to an aqueous environment, they became responsive once again and successfully released their cargo in acidic stimuli (Figure 3d).

The OPNs direct solubility in organic protic solvent, methanol and organic aprotic solvent, diethylether, was also examined. In methanol, the solubility of OPN-4, OPN-6, OPN-8, and OPN-12 was found to be 0.12, 0.15, 1.01, and 1.22 g/L, correspondingly. In ether, the OPNs' solubility was found to be 0.14, 0.17, 0.52, and 1.11 g/L for OPN-4, OPN-6, OPN-8, and OPN-12, correspondingly. Notably, the unmodified CS remains insoluble in these solvents under the same conditions.

Atomistic MDs Simulations. In order to obtain further insights into the observed experimental results, self-assembled OPN-8 polymers were modeled by atomistic MD simulations. The length of simulated OPN-8 chains was about one-third as compared to the length of experimental chains. Therefore, these chains had less binding sites, and complexes prepared from them were smaller, because fewer chains were used in the simulated complexes. Pyrene (a hydrophobic model guest molecule) and RB (a hydrophilic model guest molecule) were added to the amphiphilic copolymers simulated in either water (a polar environment) or *p*-xylene (a nonpolar environment).

Figure 4a shows a 70-monomer long polysaccharide chain (length of ∼28 nm) at a 6:1 ratio of *N*-octyl-substituted glucosamine (Gls-8) and glucosamine (Gls), simulated in water for 15 ns. In this OPN-8 chain, the helicity is caused by the presence of intramolecular hydrogen bonds between hydroxyl OH-6 and the glycosidic oxygen (Figure 4b), and steric crowding, due to the presence of *N*-octyl chain moieties within the polysaccharide (Figure 4c). The chain helicity is reflected in the particular values of the $\phi\psi$-angles ensemble (see the Methods).[25] Figure 4d shows the OPN-8 chain is even more helical (twisted) in a nonpolar *p*-xylene solvent, where a larger twisting is consistent with a ∼30% increase in the number of intramolecular hydrogen bonds (compared to water), leading to a higher compactness of the chain. Table 1 describes the number of intramolecular hydrogen bonds (n_{HB}, cut-off 3.5 Å and angle 35°), and the radius of gyration (R_G), which were used as compactness indicators for the polymeric chains. They were calculated along the simulation trajectories using VMD (Visual Molecular Dynamics) analysis scripts.[26]

DOI: 10.1021/acsami.8b12855
ACS Appl. Mater. Interfaces 2018, 10, 36711–36720

Table 1. Average Number of Intramolecular Hydrogen Bonds $\langle n_{HB} \rangle$, Average Radius of Gyration $\langle R_G \rangle$ [Å] for the Simulated OPNs

systems	in *p*-xylene (with RB guest molecules)			
	$\langle n_{HB} \rangle$	$\langle R_G \rangle$	$\langle n_{HB} \rangle$	$\langle R_G \rangle$
one chain (4a/4d)	45	81.86	61	75.75
one chain with 3 guest molecules (4e/4f)	46	80.64	67	72.06
two chains (4g/4h)	90	79.99	135	69.86
ten chains (4i/4l)	673	96.50	1177	56.04
ten chains with 48 guest molecules (4j/4n)	670	83.02	1242	56.03
	in water (with RB as guest molecules)			
	$\langle n_{HB} \rangle$	$\langle R_G \rangle$	$\langle n_{HB} \rangle$	$\langle R_G \rangle$
4j/4n in opposite solvent (4m/4k)	1161	76.12	680	84.30

When the chain was moved from water to *p*-xylene, R_G was decreased and n_{HB} was increased, in agreement with tighter chain conformations, as observed in Figure 4d.

Next, the OPN-8 chain was simulated together with three pyrene (in water) or three RB molecules (in *p*-xylene) (Figure 4e,f). In water, pyrene binds with two *N*-octyl substituents. In *p*-xylene, where the chain was more distorted, RB developed a more stable binding to it and further contributed to its deformation. After 15 ns of simulation time, the chain became slightly more deformed in both solvents within the areas where the guests resided, as evidenced by a slightly larger n_{HB} and a slightly smaller R_G. Two chains without guest molecules were also simulated in water (Figure 4g) and *p*-xylene (Figure 4h). Both chain pairs were braided (tighter intermolecular packing) analogously as individual chains.[24]

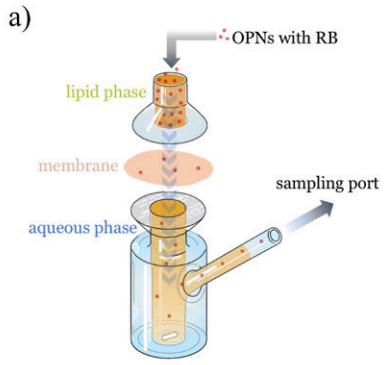
Finally, in Figure 4i–n, 10 randomly distributed polysaccharide chains, each formed by 105 monomers (6:1 ratio of Gls-8/Gls), were simulated in both solvents with/without 48 guest molecules. Figure 4i shows a rather expanded configuration of the chains self-assembled in water (60 ns). Figure 4j shows this system with 48 randomly distributed pyrene residues (60 ns), which contributed to a significant tightening of the whole assembly, in agreement with our experimental cryo-TEM images. In total, 37 guest molecules are bound to the polymer network, typically, in hydrophobic pockets formed in between adjacent substituents (see Movies 1 to 7 in the Supporting Information), causing a large collapse of the self-assembled chains. Figure 4k shows that when 48 (hydrophilic) RB guest molecules are present in a system that is solvated in water, only 5 RB molecules become encapsulated (50 ns). Figure 4l–n reveal analogous simulations performed in *p*-xylene. Figure 4l shows the self-assembled chains are highly collapsed in *p*-xylene, revealing their significant hydrophilicity (60 ns). It should not come as a surprise that only 13 (hydrophobic) guest pyrene molecules remain encapsulated in a *p*-xylene assembly (50 ns), as shown in Figure 4m. On the other hand, Figure 4n reveals that all 48 (hydrophilic) RB molecules remain encapsulated in *p*-xylene (60 ns). These observations show that the designed chains could encapsulate an active payload and potentially transfer it from an unfavorable environment to a favorable environment (aqueous solvents for hydrophilic molecules or hydrophobic solvents for hydrophobic molecules), where the active payload can be released.

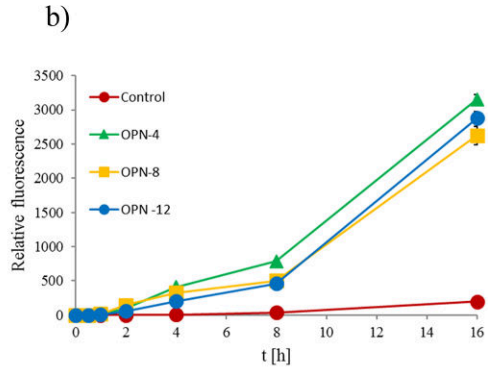
Activity Studies. *Transferring Active Agents Across a Lipid Barrier toward an Aqueous Phase.* The OPNs' phase transfer ability was demonstrated using a Franz diffusion cell,[27] which is a common in vitro model used to estimate the ability of compounds to be transferred across lipid barriers into an aqueous phase. This model is widely used in pharmacology and cosmetics for transdermal delivery studies[28] and can even be used to study cuticle penetration in plant leaves.[29] In this experiment, RB containing OPNs were dissolved in sunflower oil and allowed to permeate spontaneously across an artificial skin-like lipophilic membrane onto an aqueous solution, where their fluorescent intensity was sampled. The results show all of the inspected OPNs have successfully transported encapsulated RB across the lipophilic barrier. As a control test, it can be seen that without OPNs, RB (red) scarcely permeates across the membrane (Figure 5).

pH Stimuli Induced Release and Amplification of the Bioactivity in Encapsulated Agents. The ability of the OPNs to amplify the bioactivity of encapsulated agents was demonstrated on a wheat grains model. For this purpose, OPN-6 was prepared by coupling CS with hexanal, an antifungal aldehyde.[30] Various nature-sourced antifungal agents were then encapsulated in it (1-octanol, eugenol, thymol, oreganum oil, or tea tree oil), yielding five formulations. Wheat grains were separately exposed to these different formulations and triggered by acidic stimuli in order to activate the N-imine dynamic covalent bond. Exposure time lasted for 20 days, and the grains were then placed on potato dextrose agar (PDA) plates to promote microbial growth. Several control treatments were used: the directly added antifungal agents, a standalone hexanal (as the attached appendage in OPN-6), a standalone acidic stimuli treatment, and CS on its own. OPNs have shown to significantly amplify the antifungal activity of the encapsulated active agent, regardless of the agent type (Figure 5c, third row). These treatments had performed even better than the same active ingredients that had been added directly (Figure 5c, second row), and better than inactivated OPN formulations with encapsulated antifungal agents (Figure 5c, first row). The superior antifungal properties of the third row treatments stem from two major factors, being the effective delivery properties and the dynamic covalent bond design that allowed releasing hexanal as an auxiliary antifungal agent that laid dormant until properly triggered.

The timed cleavage process reverted the OPNs back to their original components, releasing the coupled aldehydes in addition to payload discharge. For this reason, the coupled aldehydes were not only chosen for their synthetic compatibility and introduced hydrophobicity but also for their biological properties; specifically, for their antioxidant, antimicrobial, antifungal, and antibacterial activities that are only fully expressed when the aldehydes are free molecules. The dynamic bond strategy has thus ensured a temporal inertness of these components until the opportune moment, providing the resulting delivery systems with advanced multiple biological activities. It is worth noting that the stimuli-responsive disassembly of the prepared OPNs is an optional design feature that can be easily withdrawn simply by reducing the dynamic N-imine bond to a steadier secondary amine bond.

DOI: 10.1021/acsami.8b12855
ACS Appl. Mater. Interfaces 2018, 10, 36711–36720





c)

Fungal inoculation [%]

	1-octanol	Eugenol	Thymol	Oreganum oil	Tea tree oil	Controls	Controls
OPN-6 + antifungal agent	100	100	94.3	100	100	100	Untreated
Directly added antifungal agents	92	86.8	57.4	65.3	47.6	100	Acidic stimuli
OPN-6 + antifungal agent activated by acidic stimuli	37.4	26.4	28.6	31	17.4	100	OPN-6
						44.7	Hexanal
						41	OPN-6 + acidic stimuli

Fully inoculated
No inoculation

d)

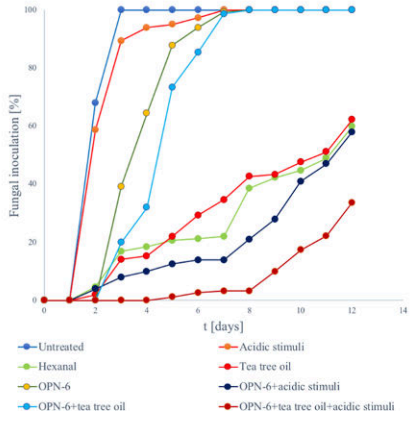


Figure 5. continued

DOI: 10.1021/acsami.8b12855
ACS Appl. Mater. Interfaces 2018, 10, 36711−36720

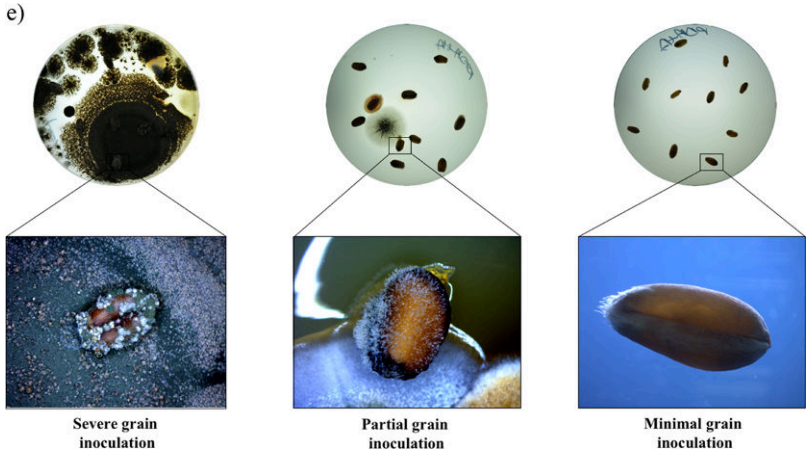


Figure 5. (a) Franz diffusion cell experiment for OPNs loaded with RB in sunflower oil. Their successful passage across a lipophilic membrane was recorded using a spectrofluorometer (b) as sampled from the aqueous phase, showing a successful stability and cross-phase transport over unencapsulated RB. (c) Fungal inoculation for all of the active agents and controls used in this experiment after 10 days of exposure time. (d) Fungal inoculation in wheat grains when treated with encapsulated tea tree oil in an OPN-6 formulation (full inhibition profiles for other formulations are accessible as shown in the Supporting Information). (e) Light microscopy enlargements of wheat grains with fungal inoculations at different stages.

CONCLUSIONS

The self-assembled polysaccharide-based OPNs exhibited a remarkable ability of auto-adjustments in various media of different polarities and a successful encapsulation of varied guest molecules within aqueous or lipid environments, enabling shuttling them through cross-phase barriers. The OPN design contains pH-responsive N-imine dynamic covalent bonds, allowing the amplification of the encapsulated agents' activity. Being a complexed macromolecule, OPNs manifest a structural plasticity and adaptiveness. Therefore, they can perform numerous architectural self-adjustments, thus providing different favorable microenvironments for various guest interactions and accommodations. This allows OPNs to deal with miscellaneous combinations of active payloads and bulk media, enabling cross-phase transport capabilities.

The presented OPNs may serve as advanced biocompatible nanoplatforms for the delivery of active agents in many fields. They are especially valuable in predicaments where the phase barrier paradigm is inescapable, such as the transdermal transfer of hydrophilic agents in medicine or cosmetics, or the delivery of nutrients across plant epidermis in agriculture.

MATERIALS AND METHODS

Materials. CS was purchased from Molekula (Munich, Germany). Butanal and octanal were purchased from Acros Organics (Geel, Belgium). Hexanal, dodecanal, acetic acid, curcumin, pyrene, HCl, chloramphenicol, thymol, 1-octanol, eugenol, and FTIR-grade potassium bromide were purchased from Sigma-Aldrich (Steinheim, Germany). RB was purchased from Fisher Chemicals (Loughborough, UK). Aluminum chloride was generously donated by Prof. Arkadi Vigalok from Tel Aviv University's School of Chemistry. Xylene (a mixture of o-, m- and p-) and ethanol were purchased from Bio-Lab (Ashkelon, Israel). Organic cold-pressed sunflower oil was purchased from Joe & Co. (Vicenza, Italy). Double deionized water (DDW) was obtained by mechanically filtering them through a Treion TS1173 column. Oreganum oil and tea tree oil were purchased from J. D. Schloss Aroma therputics Inc. Wheat grains were kindly donated by Dr. Moshe Kostyukovsky from Volcani Center's Department of Food Quality and Safety. PDA was purchased from Difco Fisher Scientific. All regents and solvents were purchased at an analytical grade or higher and were used without further purification.

Methods. *Synthetic Procedure.* CS (1.5% w/w) was dissolved in 100 mL of DDW solution that contain 0.6% v/v acetic acid, which facilitated polymer solubility, and stirred at 23 ± 1 °C for 60 min to achieve sufficient homogeneity. An aldehyde was then added at 25.1 mmol (2.85 equiv in respect to CS's amines) and the solution was stirred overnight. Solutions were then kept at 4 ± 1 °C for analyses. Modified polymer films were obtained by casting 5 mL portions of the solutions immediately after their overnight preparation into Teflon Petri dishes (5 cm in diameter) and dried at 23 ± 1 °C for an additional overnight at a relative humidity (RH) of 65 ± 2%, and the prepared films were washed with hexane to remove excess unattached aldehydes, dried for 2 h in a vacuum desiccator, and stored at −18 °C.

Determination of Degree of Deacetylation (% DD). CS's degree of deacetylation (% DD) was determined using the first derivative UV method in which the polymer is cleaved by phosphoric acid to yield its individual monomers that are inspected under UV light, and their ratio is then determined.[31] % DD was also corroborated using ^{1}H NMR scans by calculating the integral value for N-acetyl group of CS, confirmed at 94%.[32]

Gel Permeation Chromatography. Molecular weight and polydispersity index for CS were determined as 59 826 g/mol and 3.66 M_w/M_n, respectively. This was done using gel permeation chromatography (GPC) consisting of a Waters Alliance system e2695 separation module (Waters Israel), equipped with a refractive index detector, model blue 2414. The mobile phase used was a 0.02 M acetic acid/0.1 M sodium acetate buffer with an addition of 10 mL of acetic acid to the 2.5 L buffer batch (pH 4.2) under isocratic elution for 30 min at a flow rate of 0.7 mL min^{-1}. The injection volume was 20 μL, and the temperature of both the detector and columns was 30 °C. Analyses were carried out using an ultra-hydrogel column, 2000, 12 μm, 7.8 mm × 300 mm, 500−10 M (Waters). Molecular weights were determined relative to a dextran standards kit (PSS Polymer standards service GmbH, Germany) with a molecular weight range of 4400−401 000 Da. All data provided by the GPC system were collected and analyzed with the Empower 3 personal dissolution software.

Calculating the Degree of Substitution. The product films (5 mg) were dissolved in water (4 mL DDW), and acetic acid was added (100 μL) to cleave off the N-imine bond and detach the aldehydes from the polymers. The aldehydes were then extracted by an organic solvent and analyzed using a Shimadzu gas chromatography (GC) 2010 apparatus equipped with an autosampler (MPS, Gerstel, USA). Aldehyde extraction was performed by hexane (5 mL × 3) for octanal, hexanal, and dodecanal and by toluene for butanal. Three repetitions of a 1 μL organic phase sample volume were then injected to a GC

DOI: 10.1021/acsami.8b12855
ACS Appl. Mater. Interfaces 2018, 10, 36711−36720

apparatus(starting oven temperature 60 °C), holding for 1 min, followed by a temperature increase rate of 10 °C/min to 100 °C, an additional increase rate of 20 °C/min to 200 °C, and a final temperature increase rate of 10 °C/min to 280 °C holding for 3 min, with helium as the carrier gas at a flow rate of 1.3 mL/min; split, 1:50. The injection port was set at 250 °C. Analytes were separated on an Agilent VF5-ms column (30 m length, 0.25 mm i.d, 0.25 μm film thickness), and detection was made on a flame ionization detector (FID) at a set temperature of 290 °C. Shimadzu LabSolutions software was used for post-run analysis and retention times were identified at 2.03, 3.45, 6.01, and 9.76 min for butanal, hexanal, octanal, and dodecanal respectively. Obtained areas for the individual aldehydes (which had been individually calibrated using the calibration curve) indicated the amount of aldehyde per 1 mL of solution and used to find the amount of the aldehyde substituent in 1 mg of the modified film. The degree of substitution of the modified polymers was calculated as follows

$$\text{Mole of aldehyde} \div \text{mole of glucosamine units (in 1 g of modified film)}$$

The mole of aldehyde was calculated by GC analysis. The mole of Gls units in 1 g of film was calculated as $(1/161) \times 0.94$, where 161 [g/mol] is the molecular weight of the Gls unit and 0.94% is degree of deacetylation of CS.

The degree of substitution was determined as the following: 34% for OPN-4, 47% for OPN-6, 92% for OPN-8 and 3% for OPN-12.

FTIR spectra were recorded between 400 and 4000 cm^{-1} by averaging 100 scans with a 4 cm^{-1} resolution (Bruker Tensor 27 FTIR Spectrometer) using FTIR grade potassium bromide discs.

Determining CACs. *Spectrofluorometry.* CACs for the OPNs were studied with pyrene as a fluorescent probe using a previously described method.[33] Pyrene was first dissolved in absolute ethanol to obtain a 1 mM stock solution and then further diluted with various aqueous OPN solutions at varying concentrations, always yielding a final pyrene concentration of 1 μM. Fluorescence spectra of OPN samples were measured in a standard 1 cm quartz cell using a computer-controlled Shimadzu, RF-5301PC spectrofluorometer equipped with a 150W Xenon Lamp (Ushio Inc., Japan). The excitation wavelength for pyrene was 330 nm with a slit width of 3 nm, and the emission band was recorded at 360−380 nm with a slit width of 3 nm, at increments of 0.5 nm. All samples were measured at 23 ± 1 °C. All samples were measured in duplicates and each duplicate was scanned twice. CAC values were calculated as the intersection between two linear lines depicting aggregate formation dependent on concentration in solution, according to a method previously reported.[34] Additional fluorescent probes were used to demonstrate their encapsulation by aggregates, formed by the prepared OPNs. Encapsulation was identified by a change in the probes' intensities. The excitation wavelengths for RB and curcumin were 557 and 420 nm with a slit width of 3 and 1.5 nm, respectively. All spectra were obtained at increments of 0.5 nm, and performed at 23 ± 1 °C.

Dynamic Light Scattering. CAC values for the OPNs were also gauged using a Nano ZS ZEN3500 Malvern light scattering photometer equipped with a 50 mW laser at an operating wavelength of 532 nm. All measurements were conducted at 23 °C (refractive index 1.330 and viscosity 0.890 cP for water, 1.496 and 0.812 cP for xylene, respectively) with an angle detection ϑ of 173°. Samples were prepared from original reaction solutions at varying dilutions and have been vortexed prior to measurements. Each sample was measured three times, and the average serial data were calculated.

Confocal Microscopy. CLSM imaging was performed using a Leica SP8 inverted confocal microscope (Germany) with LAS-X software and an HC PL APO CS2 63×/1.20 water immersion objective. Pyrene was excited at 405 nm and emission was collected from 415 to 530 nm. RB was excited at 552 nm and emission was collected from 565 to 650 nm. Curcumin was excited at 420 nm and emission was collected from 470 to 570 nm. Fluorescent dye solutions were freshly prepared on the day of imaging (10 μM) and were also inspected separately under the microscope to ensure no contaminants were present to obtain false micro particles.

Cryo-TEM. For direct imaging using cryo-TEM, a 3 μL drop of OPN solution was placed on a glow-discharged TEM grid (300-mesh Cu grid) coated with a holey carbon film (Lacey substrate, Ted Pella Ltd.). To obtain a thin film, excess sample was blotted using filter papers, and the grid was immediately plunged into liquid ethane precooled by liquid nitrogen using Vitrobot Mark IV (FEI). The vitrified samples were examined at −177 °C using a FEI Tecnai 12 G2 TWIN TEM equipped with a Gatan 626 cold stage, and the images were recorded (4k × 4k FEI Eagle CCD camera) at 120 kV in low-dose mode. TIA (Tecnai Imaging & Analysis) software was used to record the images and to measure the diameters of the spherical assemblies. The average diameter was calculated from diameter values obtained from measuring over 200 aggregates from images of each sample.

OPN Solubilization in Lipophilic Solvents. Aqueous OPN solutions (0.5 mL of CS, OPN-4, OPN-8 or OPN-12 at a concentration of 1.5 g/mL) were added to 10 mL of a hydrophobic polar aprotic solvent (xylene) or sunflower oil. The resulting solutions were then heated to 100 °C for 30 min while stirring, in order to evaporate trace waters that were inserted with the OPNs. A fluorescent dye was then added (pyrene, RB or curcumin) at a concentration of 0.543 mM. Solutions were then filtered with a Minisart nonpyrogenic 0.22 μm filter and then further inspected analytically.

OPN Solubilization in Methanol and Ether. The 20 mg of OPN-4; OPN-6; OPN-8; OPN-12, and CS films were stirred at room temperature in 10 mL of methanol (protic solvent), and diethyl ether (aprotic solvent) overnight in order to dissolve the maximal amount of film. Then, the mixture was filtered using cotton wool to remove the nondissolved polymer species. The filtered solutions (5 mL) were transferred to weighed vials, and the organic solvents were allowed to evaporate in the hood. The vials were then put in the desiccator connected to the vacuum pump (∼50 mm Hg) to remove solvent residues and weighed. This method allowed quantifying the maximal solubility of the polymer in the specific solvent. The reported values represent an average data from three replications.

MDs Simulations. The MD simulations were performed with the NAMD[35] package using an *NPT* ensemble with P = 1 bar and T = 300 K. The systems were simulated with a Langevin dynamics, a damping constant of 1 ps^{-1} and a time step of 2 fs. Nonbonding interactions were calculated using a cutoff distance of 10 Å and long-range electrostatic interactions were calculated using the particle mesh Ewald (PME) method[36] in the presence of periodic boundary conditions. TIP3P water molecules were used in a water box. Most of the molecular force field parameters were obtained from the CHARMM general force field, except of the bond angle and the dihedral of the connection between the octyl-substituted and nonsubstituted Gls unit.[37,38] Missing parameters and partial atomic charges were calculated using HF/6-311+G(d,p) and the electrostatic potential fitted point charges using the CHELPG algorithm with polarizable continuum model (PCM) (water and *p*-xylene) by Gaussian 09 package.[39] In order to get the correct force field for extended polysaccharides, ab initio calculations of two disaccharides were performed: (1) octyl-substituted Gls with octyl-substituted Gls (Gls-8/Gls-8 disaccharide) and (2) octyl-substituted Gls with Gls (Gls-8/Gls). The connecting regions within the disaccharides were used to find the dihedrals necessary for extended chains. In order to create extended, unbranched polysaccharide chains (OPN-8) studied in the experiments, we prepared model chains formed by Gls-8 and Gls monomers combined in a 6:1 repetitive ratio. The relative orientations of the monomers in polysaccharide systems are expressed in terms of glycosidic linkage dihedral angles,[40] defined as $\phi = O_5-C_1-O-C_X^1$ and $\psi = C_1-O-C_X'-C_{[x-1]}'$ for $(1 \rightarrow x)$ linkages (Figure 4b). An energetically friendly orientation of dihedral angles yields a ψ/ϕ of −20.0/−80.31 for the system Gls-8/Gls-8 disaccharide and 21.3/−79.8 for the system Gls-8/Gls disaccharide.

Franz Diffusion Cell. The ability of the OPNs to enhance RB permeation in vitro was evaluated using a vertical static Franz

DOI: 10.1021/acsami.8b12855
ACS Appl. Mater. Interfaces 2018, 10, 36711−36720

diffusion cell apparatus (PermeGear, Inc., Hellertown, PA, USA). The lipid phase was loaded with 250 μL of the sunflower oil-based OPNs containing RB and mounted on an artificial membrane that mimics a skin-like barrier (Strat-M Membrane, Merck Millipore, Darmstadt, Germany). The receptor chamber was filled with 5 mL of phosphate buffered saline (pH 7.4), was constantly stirred (500 rpm), and maintained at 32 ± 0.5 °C. Samples (250 μL) were withdrawn from the receptor aqueous phase at six predetermined time intervals (0.5, 1, 2, 4, 8, and 16 h), and the chamber was refilled with an equivalent amount of fresh buffer solution. The rate of RB permeation was determined fluorescently (excitation at 557 nm and emission at 600 nm) using a Fluoroskan Ascent Microplate reader (Thermo Scientific). All samples were tested in triplicate repetitions.

Inhibition of Fungal Growth. Inhibition of fungal growth on wheat grains was inspected by exposing the grains (at a moisture content of 12%) to various treatments. 50 grains were added to sterile light-protected 250 mL bottles. Different additives were then inserted in smaller vials to ensure no direct contact between them and the grains. The bottles were then sealed for 20 days and kept at a controlled temperature of 30 °C with a RH of 65−70% inside the bottles. The examined treatments were: (a) untreated (no additives), (b) HCl by direct addition (5 mL, 3 M), (c) hexanal 75 μL, (d) 1-octanol 75 μL, (e) eugenol 75 μL, (f) thymol 75 μL, (g) oreganum oil 75 μL, (h) tea tree oil 75 μL, (i) CS 100 mg, (j) OPN-6100 mg, (k) OPN-6100 mg in a 5 mL HCl 3 M solution, (l) OPN-6 with encapsulated 1-octanol 100 mg, (m) OPN-6 with encapsulated 1-octanol 100 mg in a 5 mL HCl 3 M solution, (n) OPN-6 with encapsulated eugenol 100 mg, (o) OPN-6 with encapsulated eugenol 100 mg in a 5 mL HCl 3 M solution, (p) OPN-6 with encapsulated thymol 100 mg, (q) OPN-6 with encapsulated thymol 100 mg in a 5 mL HCl 3 M solution, (r) OPN-6 with encapsulated oreganum oil 100 mg, (s) OPN-6 with encapsulated oreganum oil 100 mg in a 5 mL HCl 3 M solution, (t) OPN-6 with encapsulated tea tree oil 100 mg, and (u) OPN-6 with encapsulated tea tree oil 100 mg in a 5 mL HCl 3 M solution. Following the incubation period, bottles were opened, and the grains were taken for infestation evaluation using the direct plating method. Grains were then placed in Petri dishes (ten grains per plate) containing PDA and 0.005% chloramphenicol to promote fungal growth. The plates were prepared by dissolving 39 g of PDA and 50 mg chloramphenicol in 1 L of DDW and stirred at 90 °C for 5 min for complete homogeneity. The solution was then autoclaved at 121 °C for 15 min. The number of infested grains was counted and recorded daily for 12 days. All of the treatments above were tested in triplicates.

■ ASSOCIATED CONTENT

Supporting Information

The Supporting Information is available free of charge on the ACS Publications website at DOI: 10.1021/acsami.8b12855.

This text is accompanied by electronic Supporting Information that includes FTIR spectra, CAC concentrations, spectrofluorometric scans of the OPNs with different guests in different environments, CLSM images of different OPNs with different guests in different environments, density distribution for the simulated OPNs, a list of active links, where the presented simulations can be seen, and full antimicrobial expressions of the different OPNs with various active agents (PDF)

Atomistic molecular dynamics simulation of one chain with 3 pyrene molecules in water (Figure 4e) (AVI)

Atomistic molecular dynamics simulation of 10 chains in water (Figure 4i) (AVI)

Atomistic molecular dynamics simulation of 10 chains with 48 pyrene molecules in water (Figure 4j) (AVI)

Atomistic molecular dynamics simulation of 10 chains with 48 RB molecules in water (Figure 4k) (AVI)

Atomistic molecular dynamics simulation of 10 chains in *p*-xylene (Figure 4l) (AVI)

Atomistic molecular dynamics simulation of 10 chains with 48 pyrene molecules in *p*-xylene (Figure 4m) (AVI)

Atomistic molecular dynamics simulation of 10 chains with 48 RB molecules in *p*-xylene (Figure 4n) (AVI)

■ AUTHOR INFORMATION

Corresponding Author

*E-mail: elenap@volcani.agri.gov.il.

ORCID

Petr Král: 0000-0003-2992-9027

Elena Poverenov: 0000-0003-1646-2624

Notes

The authors declare no competing financial interest.

■ ACKNOWLEDGMENTS

This research was supported by the Chief Scientist of the Israeli Ministry of Agriculture, grant no. 421-0383-18. Contribution from the Agricultural Research Organization, The Volcani Center, no 815/18. The study was also partially supported by the Ministry of Science and Technology, Israel. P.K. was supported by the NSF-DMR grant 1506886. The authors would like to thank Eduard Belausov for CLSM imaging and analysis.

■ REFERENCES

(1) Sen, S.; Han, Y.; Rehak, P.; Vuković, L.; Král, P. Computational Studies of Micellar and Nanoparticle Nanomedicines. *Chem. Soc. Rev.* **2018**, *47*, 3849.

(2) Discher, D. E.; Eisenberg, A. Polymer Vesicles. *Science* **2002**, *297*, 967−973.

(3) Jiang, W.; Zhou, Y.; Yan, D. Hyperbranched Polymer Vesicles: from Self-Assembly, Characterization, Mechanisms, and Properties to Applications. *Chem. Soc. Rev.* **2015**, *44*, 3874−3889.

(4) Soppimath, K. S.; Aminabhavi, T. M.; Kulkarni, A. R.; Rudzinski, W. E. Biodegradable Polymeric Nanoparticles as Drug Delivery Devices. *J. Controlled Release* **2001**, *70*, 1−20.

(5) Kamaly, N.; Yameen, B.; Wu, J.; Farokhzad, O. C. Degradable Controlled-Release Polymers and Polymeric Nanoparticles: Mechanisms of Controlling Drug Release. *Chem. Rev.* **2016**, *116*, 2602−2663.

(6) Joye, I. J.; McClements, D. J. Biopolymer-based Delivery Systems: Challenges and Opportunities. *Curr. Top. Med. Chem.* **2016**, *16*, 1026−1039.

(7) Malviya, R.; Sharma, P. K.; Dubey, S. K. Modification of Polysaccharides: Pharmaceutical and Tissue Engineering Applications with Commercial Utility (patents). *Mater. Sci. Eng. C* **2016**, *68*, 929−938.

(8) Wolfrum, C.; Shi, S.; Jayaprakash, K. N.; Jayaraman, M.; Wang, G.; Pandey, R. K.; Rajeev, K. G.; Nakayama, T.; Charrise, K.; Ndungo, E. M.; Zimmermann, T.; Koteliansky, V.; Manoharan, M.; Stoffel, M. Mechanisms and Optimization of *in vivo* Delivery of Lipophilic siRNAs. *Nat. Biotechnol.* **2007**, *25*, 1149−1157.

(9) Gu, L.; Faig, A.; Abdelhamid, D.; Uhrich, K. Sugar-Based Amphiphilic Polymers for Biomedical Applications: from Nanocarriers to Therapeutics. *Acc. Chem. Res.* **2014**, *47*, 2867−2877.

(10) Prausnitz, M. R.; Langer, R. Transdermal Drug Delivery. *Nat. Biotechnol.* **2008**, *26*, 1261−1268.

(11) Schoellhammer, C. M.; Blankschtein, D.; Langer, R. Skin Permeabilization for Transdermal Drug Delivery: Recent Advances and Future Prospects. *Expet Opin. Drug Deliv.* **2014**, *11*, 393−407.

(12) Kakkar, A.; Traverso, G.; Farokhzad, O. C.; Weissleder, R.; Langer, R. Evolution of Macromolecular Complexity in Drug Delivery Systems. *Nat. Rev. Chem.* **2017**, *1*, 0063.

DOI: 10.1021/acsami.8b12855
ACS Appl. Mater. Interfaces 2018, 10, 36711−36720

(13) Fernández, V.; Eichert, T. Uptake of Hydrophilic Solutes Through Plant Leaves: Current State of Knowledge and Perspectives of Foliar Fertilization. *Crit. Rev. Plant Sci.* **2009**, *28*, 36−68.
(14) Kumar, M. N. V. R.; Muzzarelli, R. A. A.; Muzzarelli, C.; Sashiwa, H.; Domb, A. J. Chitosan Chemistry and Pharmaceutical Perspectives. *Chem. Rev.* **2004**, *104*, 6017−6084.
(15) Park, J. H.; Saravanakumar, G.; Kim, K.; Kwon, I. C. Targeted Delivery of Low Molecular Drugs Using Chitosan and Its Derivatives. *Adv. Drug Deliv. Rev.* **2010**, *62*, 28−41.
(16) Battinelli, L.; Daniele, C.; Cristiani, M.; Bisignano, G.; Saija, A.; Mazzanti, G. *In vitro* Antifungal and Anti-Elastase Activity of Some Aliphatic Aldehydes from *Olea Europaea L*. Fruit. *Phytomedicine* **2006**, *13*, 558−563.
(17) Rutenberg, R.; Golden, G. I.; Cohen, Y.; Kleiman, P.; Poverenov, E. Investigation of substituent effect in modified nature-sourced polymers: rational side chain engineering to control yield, design and properties. *ACS Omega* **2018**, *3*, 12841−12850.
(18) Setter, O.; Livney, Y. D. The effect of sugar stereochemistry on protein self-assembly: the case of *β*-casein micellization in different aldohexose solutions. *Phys. Chem. Chem. Phys.* **2015**, *17*, 3599−3606.
(19) Maheshwari, R. K.; Singh, A. K.; Gaddipati, J.; Srimal, R. C. Multiple Biological Activities of Curcumin: A Short Review. *Life Sci.* **2006**, *78*, 2081−2087.
(20) Minkenberg, C. B.; Florusse, L.; Eelkema, R.; Koper, G. J. M.; van Esch, J. H. Triggered Self-Assembly of Simple Dynamic Covalent Surfactants. *J. Am. Chem. Soc.* **2009**, *131*, 11274−11275.
(21) Jackson, A. W.; Fulton, D. A. Making Polymeric Nanoparticles Stimuli-Responsive with Dynamic Covalent Bonds. *Polym. Chem.* **2013**, *4*, 31−45.
(22) Fadida, T.; Selilat-Weiss, A.; Poverenov, E. N-hexylimine-chitosan, a biodegradable and covalently stabilized source of volatile, antimicrobial hexanal. Next generation controlled-release system. *Food Hydrocolloids* **2015**, *48*, 213−219.
(23) Jia, Z.; shen, D.; Xu, W. Synthesis and Antibacterial Activities of Quaternary Ammonium Salt of Chitosan. *Carbohydr. Res.* **2001**, *333*, 1−6.
(24) Betschart, H. R.; Jondorf, W. R.; Bickel, M. H. Differences in Adipose Tissue Distribution of Basic Lipophilic Drugs Between Intraperitoneal and Other Routes of Administration. *Xenobiotica* **1988**, *18*, 113−121.
(25) Yoshioka, H.; Nonaka, K.-i.; Fukuda, K.; Kazama, S. Chitosan-Derived Polymer-Surfactants and Their Micellar Properties. *Biosci. Biotechnol. Biochem.* **1995**, *59*, 1901−1904.
(26) Humphrey, W.; Dalke, A.; Schulten, K. VMD: Visual molecular dynamics. *J. Mol. Graphics* **1996**, *14*, 33−38.
(27) Ng, S.-F.; Rouse, J. J.; Sanderson, F. D.; Meidan, V.; Eccleston, G. M. Validation of a Static Franz Diffusion Cell System for *In vitro* Permeation Studies. *AAPS PharmSciTech* **2010**, *11*, 1432−1441.
(28) Liebenberg, W.; Engelbrecht, E.; Wessels, A.; Devarakonda, B.; Yang, W.; De Villiers, M. M. A Comparative Study of the Release of Active Ingredients from Semisolid Cosmeceuticals Measured with Franz, Enhancer or Flow-Through Cell Diffusion Apparatus. *J. Food Drug Anal.* **2004**, *12*, 19−28.
(29) Kierstan, K. T. E.; Beezer, A. E.; Mitchell, J. C.; Hadgraft, J.; Raghavan, S. L.; Davis, A. F. UV-Spectrophotometry Study of Membrane Transport Processes with a Novel Diffusion Cell. *Int. J. Pharm.* **2001**, *229*, 87−94.
(30) Kubo, A.; Lunde, C. S.; Kubo, I. Antimicrobial Activity of the Olive Oil Flavor Compounds. *J. Agric. Food Chem.* **1995**, *43*, 1629−1633.
(31) Wu, T.; Zivanovic, S. Determination of the Degree of Acetylation (DA) of Chitin and Chitosan by an Improved First Derivative UV Method. *Carbohydr. Polym.* **2008**, *73*, 248−253.
(32) Hirai, A.; Odani, H.; Nakajima, A. Determination of degree of deacetylation of chitosan by 1H NMR spectroscopy. *Polym. Bull.* **1991**, *26*, 87−94.
(33) Binana-Limbele, W.; Zana, R. Fluorescence Probing of Microdomains in Aqueous Solutions of Polysoaps. 1. Use of Pyrene to Study the Conformational State of Polysoaps and Their Comicellization with Cationic Surfactants. *Macromolecules* **1987**, *20*, 1331−1335.
(34) Topel, Ö.; Çakır, B. A.; Budama, L.; Hoda, N. Determination of critical micelle concentration of polybutadiene-block-poly-(ethyleneoxide) diblock copolymer by fluorescence spectroscopy and dynamic light scattering. *J. Mol. Liq.* **2013**, *177*, 40−43.
(35) Phillips, J. C.; Braun, R.; Wang, W.; Gumbart, J.; Tajkhorshid, E.; Villa, E.; Chipot, C.; Skeel, R. D.; Kalé, L.; Schulten, K. Scalable Molecular Dynamics with NAMD. *J. Comput. Chem.* **2005**, *26*, 1781−1802.
(36) Darden, T.; York, D.; Pedersen, L. Particle mesh Ewald: An N·log(N) method for Ewald sums in large systems. *J. Chem. Phys.* **1993**, *98*, 10089−10092.
(37) Vanommeslaeghe, K.; Raman, E. P.; MacKerell, A. D., Jr. Automation of the CHARMM General Force Field (CGenFF) II: Assignment of Bonded Parameters and Partial Atomic Charges. *J. Chem. Inf. Model.* **2012**, *52*, 3155−3168.
(38) Vanommeslaeghe, K.; MacKerell, A. D., Jr. Automation of the CHARMM General Force Field (CGenFF) I: Bond Perception and Atom Typing. *J. Chem. Inf. Model.* **2012**, *52*, 3144−3154.
(39) Frisch, M. J.; Trucks, G. W.; Schlegel, H. B.; Scuseria, G. E.; Robb, M. A.; Cheeseman, J. R.; Scalmani, G.; Barone, V.; Petersson, G. A.; Nakatsuji, H.; Li, X.; Caricato, M.; Marenich, A.; Bloino, J.; Janesko, B. G.; Gomperts, R.; Mennucci, B.; Hratchian, H. P.; Ortiz, J. V.; Izmaylov, A. F.; Sonnenberg, J. L.; Williams-Young, D.; Ding, F.; Lipparini, F.; Egidi, F.; Goings, J.; Peng, B.; Petrone, A.; Henderson, T.; Ranasinghe, D.; Zakrzewski, V. G.; Gao, J.; Rega, N.; Zheng, G.; Liang, W.; Hada, M.; Ehara, M.; Toyota, K.; Fukuda, R.; Hasegawa, J.; Ishida, M.; Nakajima, T.; Honda, Y.; Kitao, O.; Nakai, H.; Vreven, T.; Throssell, K.; Montgomery, J. A., Jr.; Peralta, J. E. . .; Ogliaro, F.; Bearpark, M.; Heyd, J. J.; Brothers, E.; Kudin, K. N.; Staroverov, V. N.; Keith, T.; Kobayashi, R.; Normand, J.; Raghavachari, K.; Rendell, A.; Burant, J. C.; Iyengar, S. S.; Tomasi, J.; Cossi, M.; Millam, J. M.; Klene, M.; Adamo, C.; Cammi, R.; Ochterski, J. W.; Martin, R. L.; Morokuma, K.; Farkas, O.; Foresman, J. B.; Fox, D. J. *Gaussian 09*; Gaussian, Inc.: Wallingford CT, 2016.
(40) Pérez, S.; Kouwijzer, M.; Mazeau, K.; Engelsen, S. B. Modeling Polysaccharides: Present Status and Challenges. *J. Mol. Graph.* **1996**, *14*, 307−321.

DOI: 10.1021/acsami.8b12855
ACS Appl. Mater. Interfaces 2018, 10, 36711−36720